

Micro-cantilever Testing to Evaluate the Mechanical Properties of Thermal Barrier Coatings

Dong Liu^{1,2,*}, James Brown³ and Peter E J Flewitt^{1,3,b}

¹Interface Analysis Centre, University of Bristol, Bristol, BS2 8BS, UK

²Department of Mechanical Engineering, University of Bristol, Bristol, BS8 1TR, UK

³School of Physics, HH Wills Laboratory, University of Bristol, Bristol, BS8 1TL, UK

[*Dong.Liu@bristol.ac.uk](mailto:Dong.Liu@bristol.ac.uk)

Keywords: micro-cantilever testing, thermal barrier coating, fracture strength, superalloy

Abstract. In this paper, the application of a novel micro-scale mechanical testing technique in multi-layered (7 wt% yttria stabilized zirconia/alumina/NiCoCrAlY) thermal barrier coating system is described. A force measurement system has been introduced into a FEI Helios Dualbeam FIB/SEM workstation to allow the fabrication and testing of micro-scale cantilever beams subject to bend loading. These micro-cantilever specimens created by Ga ion milling were tested in-situ. The beams were produced at various locations to provide results for the TC, TC/BC interface and the BC. As-sprayed TBC samples were tested. This allows, for example, the non-linear elastic behaviour of the ceramic layer as well as the interface flexural strength to be evaluated. The results are compared and analysed with data obtained by nano-indentation. In addition, in-situ fractography was undertaken on the fracture surfaces to aid interpretation of the fracture data. The results are discussed with respect to the underlying fracture mechanisms.

Introduction

Thermal barrier coatings (TBCs) have been used extensively on first stage blades and vanes of advanced land-based gas turbines or aero engines to protect the underlying metallic substrate from oxidation and extreme operating temperatures [1]. TBCs normally consist of three layers: an outer ceramic top coat (TC); a metallic bond coat (BC) providing good adherence for the ceramic coating and the substrate. In addition, a thermally grown oxide (TGO) develops between the ceramic coating and the bond coat during exposure to the service temperature. The stability and durability of this multilayer system remains a critical issue for the further development of this coating. The mechanical properties like elastic modulus and fracture toughness of individual layers, bonding strength of the interfaces, and the strain tolerance of each layer are crucial when interpreting the response of the system under the stressed condition and the failure mechanism analysis after thermal exposure [1]. It is also recognized that crack propagation between ceramic and metal interface is of importance [2, 3]. To date there have been only limited studies of the fracture toughness and the flaw types that dictate the fracture resistance of coatings [4]. Studies that address coating flaws are needed before problems can be adequately analysed [2-4]. The mechanical properties of each layer and the associated interfaces need to be quantitatively determined.

In the case of brittle ceramic coatings, the mechanical properties are often measured using indentation techniques [2,5,6,7], Brillouin scattering [8], finite element simulations [9] etc. For thin coatings the metal substrate plays an important role in the interpretation of the indentation data, however, by considering both the loading and unloading response of the indentation data it is possible to measure both the hardness and elastic modulus. There is a need to take into account the interaction of the complex and non-uniform stress distribution formed under the indent with the microstructure [5]. Micro-scale tests have been used for a number of years, particularly when prepared by ion milling. However, in general, they have

been applied to evaluating the properties of selected regions of what may be classed as bulk materials [5-7]. In this paper, the micro-scale testing is extended to the investigation of air-plasma sprayed brittle ceramic coatings. The preparation of the specimens was undertaken using a dualbeam focused ion beam workstation, and the mechanical tests were carried out in-situ using a force loading and readout system. It is possible to view the specimen throughout the test as the mechanical loading is applied.

Experimental

Instrument The experimental arrangement for mechanical testing is a combination of a FEI Helios NanoLab 600i Dualbeam workstation and a compact force measurement system provided by Kleindiek. This allows in-situ loading and read-out of the applied force. The dualbeam workstation provides the capability for ion beam milling, in-situ scanning electron microscopic (SEM) imaging and 3D movements of the force sensor through a micromanipulator. Applying a force to the sensor causes the resistance change of the piezoelectric sensor which can be converted into force (μN) by the installed software. Before commencing measurements, a calibration of the force sensor is carried out by loading a standard spring of known elastic modulus embedded in the system to provide resistance conversion references and a zero load reading. The loading/unloading process and the corresponding deflection of the micro-scale specimens are recorded in terms of SEM imaging, and this is used for post-processing and measurements of the deflections.

Specimens Samples with a curved geometry designed to simulate key features of coated blade were used. Each comprised a superalloy substrate (CMSX4) with air plasma sprayed (APS) 7 wt.% Y_2O_3 -stabilised ZrO_2 (YSZ) applied onto an Amdry 995 bond coat deposited using high velocity oxygen fuel (HVOF). The thickness of the TBC varied with position around the specimen from $130\ \mu\text{m}$ to $230\ \mu\text{m}$. A typical cross-section of the TBC system is shown in Fig. 1a. The TC which is $\sim 200\ \mu\text{m}$ thick comprises lamellar splats, micro-scale air pores and defects. The interfaces, TC/TGO and TGO/BC, are undulating with a variable thickness of TGO.

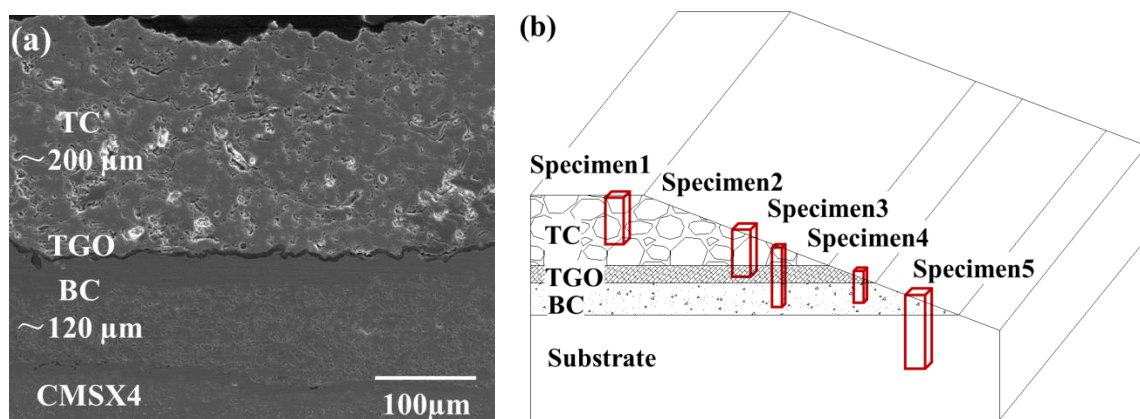


Fig. 1 The TBC system (a) typical cross-section for specimen that has been oxidised for 100 hours at 925°C and (b) creation of micro-cantilever specimen at preferred locations on tapered surface

The application of this micro-scale testing on TBC system is to measure the mechanical properties of the TC, the TC/TGO interface, the TGO/BC interface and the BC. Preparation of the micro-cantilever specimens from the TC is straightforward ion milling. But this becomes more complex for the TC/TGO or TGO/BC interfaces which are below the $\sim 200\ \mu\text{m}$ TC. Therefore, the TBC system is pre-tapered at 20° to the horizontal to create a smooth transition from the TC to the TGO and BC, Fig. 1(b), so that micro-cantilever specimens

containing the preferred features can be created (specimen 1 for TC, specimen 2 for TC/TGO, specimen 3 for TC/TGO/BC, specimen 4 for BC/substrate and specimen 5 for BC/substrate interface). The interface of BC/substrate is not the interface usually associated with failure since this is good adherence and therefore fracture resistance together with a good match between the thermal expansion coefficients. It is still possible to evaluate the properties of this interface and compare with the fragile interfaces such as TC/TGO and TGO/BC.

The production sequence of the micro-cantilever beams is summarised in Fig. 2. Fig. 2a shows the top view of the TC surface and the milling pattern is demonstrated (area: $30 \times 35 \mu\text{m}$). The locations of the micro-cantilever specimens are chosen to be close to the edge so that: (i) the force sensor has easy access to the specimen and (ii) during loading the side deflection of the beam can be recorded by SEM imaging. The desired shape of the micro-cantilever is $2 \times 2 \times 10 \mu\text{m}$. For the first step, the milling patterns produces a beam with a cross-section of $\sim 5 \times 5 \mu\text{m}$ and a length of ~ 6 to $8 \mu\text{m}$. However, due to the fact that the intensity of the focused ion beam has a Gaussian profile, milling to this depth causes tapering of the specimens, Fig. 2b. Further cleaning cross-section milling is applied after tilting the micro-cantilever specimen by an angle, θ , approximately the angle of taper. This procedure is applied to all the four sides of each micro-cantilever until a parallel geometry is achieved. The completed specimen, Fig. 2c, is surrounded by a space of ~ 15 to $20 \mu\text{m}$ between the micro-cantilever and the mainbody to allow adequate deflection during testing.

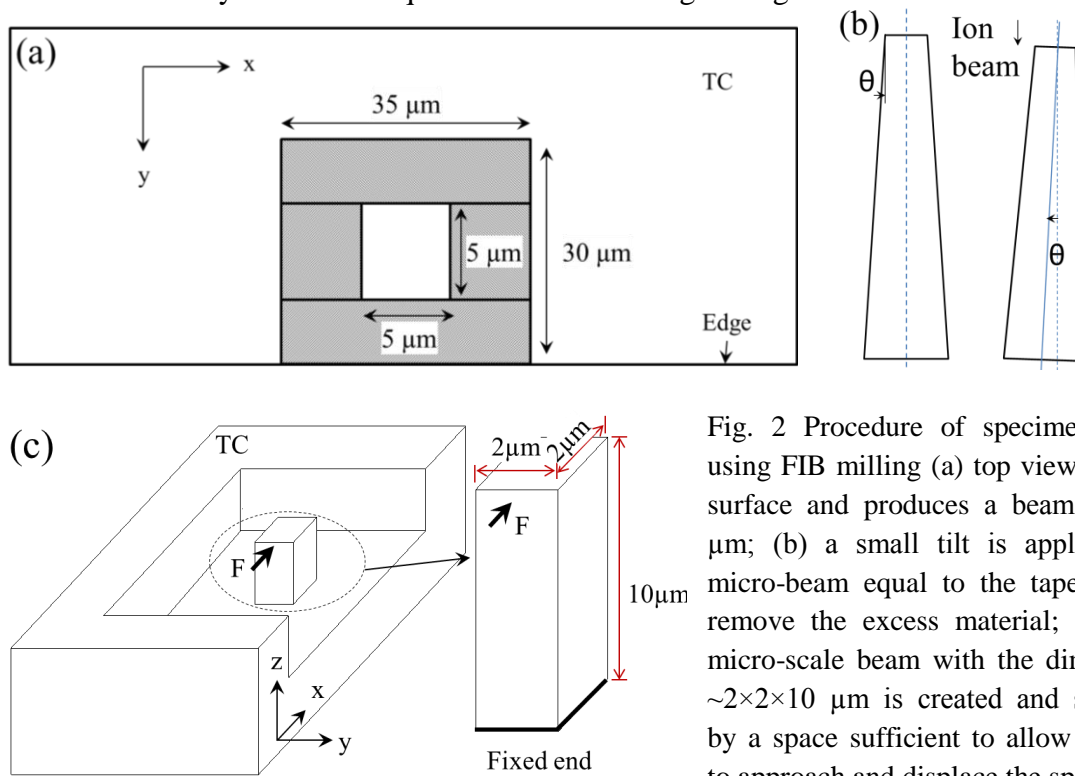


Fig. 2 Procedure of specimen creation using FIB milling (a) top view of the TC surface and produces a beam of $5 \times 5 \times 8 \mu\text{m}$; (b) a small tilt is applied to the micro-beam equal to the taper angle to remove the excess material; (c) a final micro-scale beam with the dimension of $\sim 2 \times 2 \times 10 \mu\text{m}$ is created and surrounded by a space sufficient to allow the sensor to approach and displace the specimen.

Calculations The definition of the parameters are shown in Fig. 3 where F is the applied force (μN), δ is the deflection (μm), L is the length (μm) and a is the side width of the square-sectioned micro-cantilever (a is averaged over the length of the beam). All the micro-cantilevers tested showed small deflection ($\delta/L < 5\%$), therefore the elastic modulus, E , is given by

$$E = \frac{FL^3}{3\delta I} \quad (1)$$

Where I is the moment of inertia of the beam cross-section in the case of square beam $I = \frac{a^4}{12}$. The critical fracture toughness, K_{IC} , of the tested material can be calculated by

$$K_{IC} = 1.12\sigma_f\sqrt{\pi c} \quad (2)$$

Where c is the crack length, and σ_f is the stress for tensile bending when

$$\sigma_f = \frac{FLy}{I} \quad (3)$$

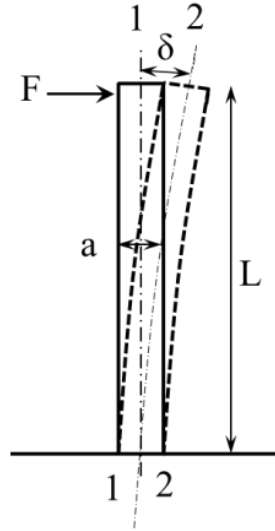


Fig. 3 Micro-cantilever specimen with applied force F . Other labels defined in the text.

Results and Discussion

In this paper we consider only the properties of the TC and TC/BC interface in as-coated APS-TBC as an example of the application of the testing method.

Mechanical Properties of TC A series of micro-cantilever specimens from the TC have been created. One example is shown in Fig. 4 with a pre-existed external flaw ($\sim 0.1 \mu\text{m}$) which is visible at one end of the splat boundary. The top of the beam is $\sim 2 \mu\text{m}$, a slight taper is present so that the base of the beam is $\sim 2.2 \mu\text{m}$. The force-deflection curve is shown in Fig. 4b and fracture occurred when the force reached $\sim 301 \mu\text{N}$. The fractured surface revealed an amorphous phase at the splat boundary which was in contact with the upper half of the beam before fracture, Fig. 4c. A detailed check of the fractured surface gives an equivalent crack area of $2 \times 1 \mu\text{m}^2$, Fig. 4d. In this figure, the large grains of YSZ ($\sim 0.8 \mu\text{m}$) can be observed which are different from the upper side of the beam with grains of sub-micrometre size. The tensile stress at fracture, σ_f , is $\sim 3.6 \text{ GPa}$, and the elastic modulus of this particular beam is $\sim 43 \text{ GPa}$. Since this micro-cantilever contains obvious defects, we define the elastic modulus obtained from the loading curve as 'equivalent modulus' which represents the entire compliance of the beam. This value is of the same magnitude as measured from macroscopic tests (10 to 100 GPa [8-12]) for as-coated TC. It should be noted that inhomogeneous and anisotropic microstructures are introduced into the TC by plasma spraying and these lead to scatter for the elastic modulus and a direction-dependency [8].

Based on the measurements derived from the experiments, the value of K_{IC} calculated for the micro-cantilever specimens is $\sim 5.05 \text{ MPa}\sqrt{\text{m}}$, which is at the higher end in the range of the reported values obtained from macroscopic tests which are in the range of 2 to 5 $\text{MPa}\sqrt{\text{m}}$ [13]; but some low values of $0.7 \text{ MPa}\sqrt{\text{m}}$ are reported [12]. However, the amorphous phase

is observed which was previously in good contact with sub-micrometre scale grains, and this may contribute to the larger fracture toughness when compared with these macroscopic values.

The force-deflection curves in this case showed a linear response until $\sim 200 \mu\text{N}$ but a slight non-linearity afterwards until the abrupt fracture. The strain was calculated by measuring the extension of the neutral line of the beam at load-free state and at the force $\sim 200 \mu\text{N}$ and that before fracture. It was found that a strain of $\sim 0.156\%$ was where the non-linear response starts and 0.261% before fracture. Compared with the reported tensile strain, 0.124% , up to which the TC showed a linear response [14] and the failure strain of 0.196% [15] in macroscopic tests, the values obtained in this contribution are larger in both cases. This is understandable since the small size of the specimen excluded the effects of other defects and the interactions between those defects in the mechanical behaviour of the sampled material.

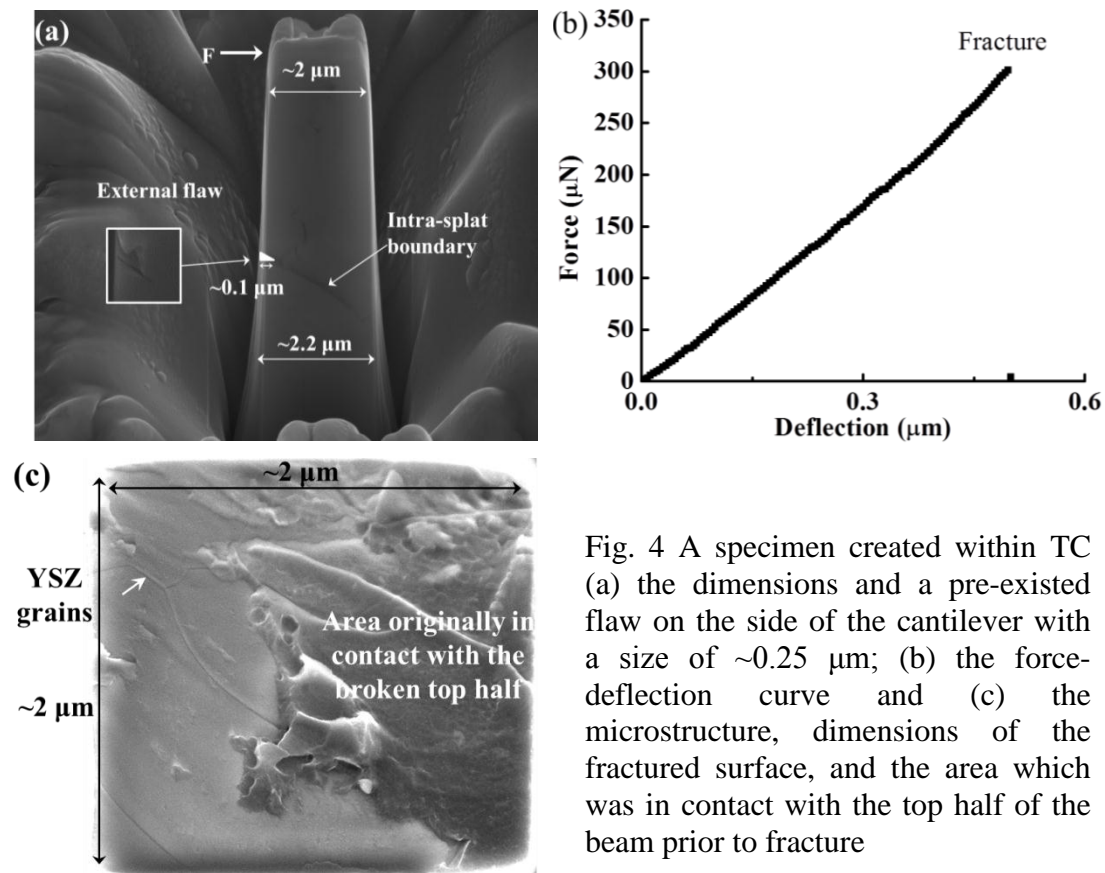


Fig. 4 A specimen created within TC (a) the dimensions and a pre-existent flaw on the side of the cantilever with a size of $\sim 0.25 \mu\text{m}$; (b) the force-deflection curve and (c) the microstructure, dimensions of the fractured surface, and the area which was in contact with the top half of the beam prior to fracture

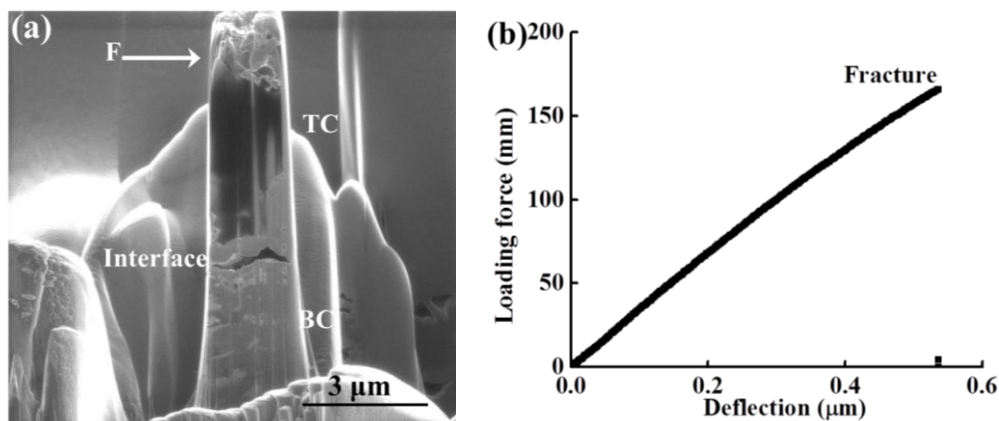


Fig. 5 (a) The micro-cantilever specimen containing the TC/BC interface and (b) the force-deflection curve

In addition to the fracture toughness of the splat interfaces, this test provides the flexural strength of the TC/BC interface, which is an important fracture parameter for brittle coatings. A flexural strength of $\sim 25 \pm 8$ MPa was derived for this as-coated material, which is close to values obtained from macroscopic tests of 30 to 40 MPa [16]. It is noteworthy that the value varies with the contact and undulation conditions between the TC and BC.

Challenges Compared with the micro-cantilever specimens created by FIB milling on many bulk metals, these specimens are produced in APS-TBCs that contain defects. The milling rate of the ion beam is modified by the localised grain size and orientation of the YSZ as shown in Fig. 6. Fig. 6a is a polished cross-section of as-coated APS-TBC with a finish of ~ 1 μm . Etching calibration was carried out using a current of 70 pA under a voltage of 30 KV to create a 20×10 μm trench on the APS-TBC and on silicon for comparison. The etched depth at this position contained a typical splat boundary in the APS-TBC and the etched depth is non-uniform depth, Fig. 6b. By comparison, the etching depth in silicon is smooth and uniform with only a slight taper at the edges, Fig. 6c. The different etching rates with location in the APS-TBC add the difficulty in creating micro-cantilever specimens with repeatable dimensions.

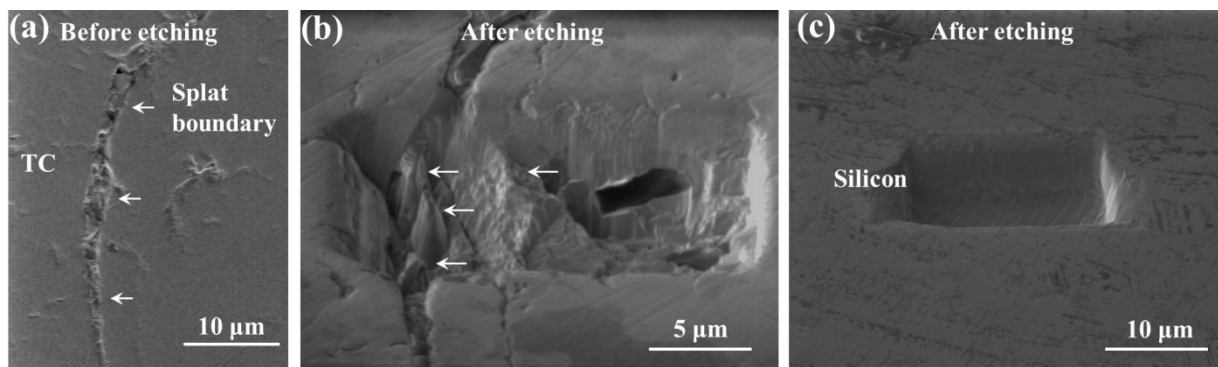


Fig. 6 (a) The polished cross-section of as-coated APS-TBC with a finish of 1 μm ; (b) the non-uniform morphology of the etched trench and (c) the etched trench on single crystal silicon using the same etching parameters for the ion beam.

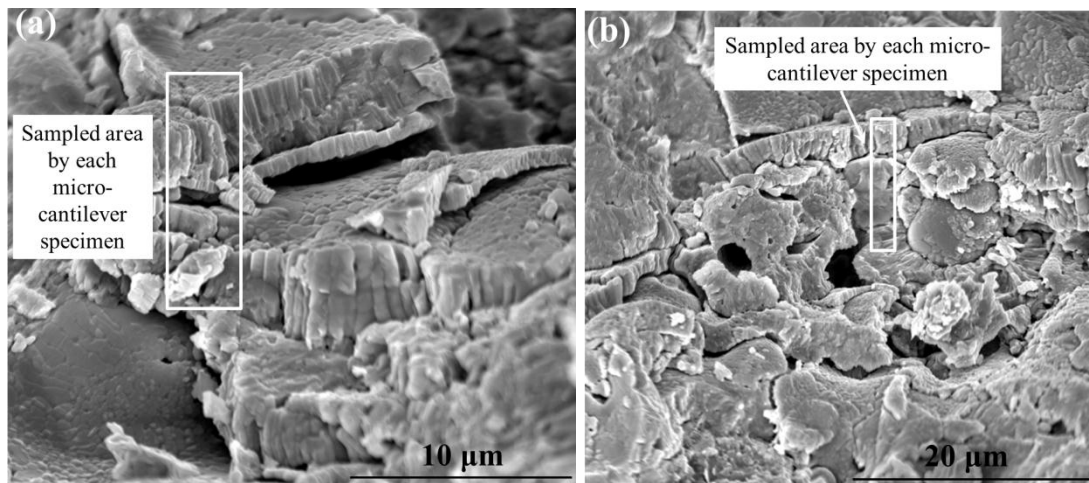


Fig. 7 SEM images of thermally exposed TBC specimens showing (a) lamellar structure of the TC and (b) complex structure comprising defects, pores and unmelt YSZ particles

The APS-TBC is composed of splats (~ 3 μm in thickness and ~ 50 μm in length), and layers of columnar grains that are formed within each splat during cooling after deposition, Fig. 7.

As a consequence, the number of the grains contained within each micro-cantilever specimen needs to be considered when interpreting the acquired data. In the thermally exposed TBC, Fig. 7a, the splat boundaries are spatially separated, in addition, there are pores present that are formed during the deposition of the TC. The size of the TBC micro-cantilever specimen is shown in each image that transversely samples ~ 30 to ~200 columnar grains and vertically samples at least one interface/boundary. This allows the examination of a particular unique interface in a given micro-cantilever specimen and excludes the effects from adjacent interfaces/cracks/defects. However, there are cases where two or more interfaces have been sampled and the force-deflection curves showed steps during loading and unloading which manifest the interactions and relative strength of the two interfaces.

Conclusion

The application of micro-cantilever tests on APS-TBC system has proved to be a reliable approach to determine the local mechanical properties and the microstructures in coated materials. The fracture toughness, elastic modulus, flexural strength calculated from the experimental data are consistent with reported values for bulk materials.

Acknowledgement

We would like to acknowledge the support of The Energy Programme, which is a Research Councils UK cross council initiative led by EPSRC and contributed to by ESRC, NERC, BBSRC and STFC, and specifically the Supergen initiative (Grants GR/S86334/01 and EP/F029748) and the following companies; Alstom Power Ltd., Doosan Babcock, E.ON, National Physical Laboratory, Praxair Surface Technologies Ltd, QinetiQ, Rolls-Royce plc, RWE npower, Siemens Industrial Turbomachinery Ltd. and Tata Steel, for their valuable contributions to the project.

References

- [1] X. Q. Cao, R. Vassen and D. Stoeber: J. Eur. Ceram. Soc. Vol. 24 (2004), p. 1.
- [2] N. A. Fleck, J. W. Hutchinson and S. Zhigang: Int. J. Solids. Struct. Vol. 27 (1991), p. 1683.
- [3] J. H. Kim and S. B. Lee: Theor. Appl. Fract. Mec. Vol. 30 (1998), p. 27.
- [4] A. G. Evans, G. B. Crumley and R. E. Demaray: Oxid. Met. Vol. 20 (1983), p. 193.
- [5] K. J. Hemker and W. N. Sharpe: Annu. Rev. Mater. Res. Vol. 37 (2007), p. 93.
- [6] M. Hopcroft, T. Kramer, G. Kim, K. Takashima, Y. Higo, D. Moore and J. Brugger: Fatigue. Fract. Eng. Mater. Struct. Vol. 28 (2005), p. 735.
- [7] D. Di Maio and S. G. Roberts: J. Mater. Res. Vol. 20 (2005), p. 299.
- [8] A. Vasinonta and J. L. Beuth: Eng. Fract. Mech. Vol. 68 (2001), p. 843.
- [9] D. Zhu and R. Miller: J. Therm. Spray. Techn. Vol. 9 (2000), p. 175.
- [10] B. Siebert, C. Funke, R. Vaßen and D. Stöver: J. Mater. Process. Tech. Vol. 92–93 (1999), p. 217.
- [11] J. A. Thompson and T. W. Clyne: Acta Mater. Vol. 49 (2001), p. 1565.
- [12] A. Rabiei and A. G. Evans: Acta Mater. Vol. 48 (2000), p. 3963.
- [13] Y. Yamazaki, S. I. Kuga and T. Yoshida: Acta Metall. Sin. (Engl. Lett.) Vol. 24 (2011), p. 109.
- [14] L. Qian, S. J. Zhu, Y. Kagawa and T. Kubo: Surf. Coat. Tech. Vol. 173 (2003), p. 178.
- [15] J.T. Demasi, K.D. Sheffler and M. Ortiz, "*Thermal Barrier Coating Life Prediction Model Development, Phase I Final Report*", (1989), p. 1.
- [16] D. M. Zhu, S. R. Choi and R. A. Miller, in: *The 106th Annual Meeting & Exposition to The American Ceramic Society*, American Ceramic Society, Indiana Convention Center & RCA Dome, Indiana (2004).